RSC Advances

PAPER

View Article Online
View Journal | View Issue

Cite this: *RSC Adv.*, 2023, **13**, 29568

Structure-directing role of CH···X (X = C, N, S, Cl) interactions in three ionic cobalt complexes: X-ray investigation and DFT study using QTAIM Vr predictor to eliminate the effect of pure Coulombic forces†

Susovan Bera,[a] Sudip Bhunia,[a] Rosa M. Gomila,[b] Michael G. B. Drew,[c] Antonio Frontera *[b] and Shouvik Chattopadhyay *[a]

Three cobalt complexes, namely $[Co^{III}(HL^1)_2(N_3)_2]ClO_4$ (**1**), $[Co^{III}(L^2)(HL^2)(N_3)]ClO_4 \cdot 1.5H_2O$ (**2**), and $[Co^{III}(L^3)(HL^3)(NCS)]_2$ $[Co^{II}Cl_2(NCS)_2]$ (**3**), where HL^1 = 2-(3-(dimethylamino)propyliminomethyl)-6-methoxyphenol, HL^2 = 2-(2-(dimethylamino)ethyliminomethyl)-4,6-dichlorophenol, and HL^3 = 2-(2-(dimethylamino)ethyliminomethyl)-6-methoxyphenol, as potential tridentate N_2O-donor Schiff base ligands, were synthesized and characterized using elemental analysis, IR and UV-vis spectroscopy, and single-crystal X-ray diffraction studies. All three were found to be monomeric ionic complexes. Complex **1** crystallizes in the orthorhombic space group *Pbcn*, whereas both complexes **2** and **3** crystallize in triclinic space groups, $P\bar{1}$. Further, **1** and **2** are cationic complexes of octahedral cobalt(III) with perchlorate anions, whereas complex **3** contains a cationic part of octahedral cobalt(III) and an anionic part of tetrahedral cobalt(II). Hydrogen-bonding interactions involving aromatic and aliphatic CH bonds as H-bond donors and the pseudo-halide co-ligands as H-bond acceptors were established, which are important aspects governing the X-ray packing. These interactions were analyzed theoretically using the quantum theory of atoms in molecules (QTAIM) and non-covalent interaction plot (NCI plot) analyses. Moreover, energy decomposition analysis (EDA) was performed to analyze the stabilization of the complexes in terms of the electrostatic, dispersion, and correlation forces.

Received 8th June 2023
Accepted 22nd September 2023

DOI: 10.1039/d3ra03828a

rsc.li/rsc-advances

Introduction

Schiff bases have long been widely used as versatile ligands for the synthesis of different transition and non-transition metal complexes with potential application in bioinorganic chemistry, opto-electronics and magnetism, catalysis, separation and encapsulation, hydrometallurgy, drug designing, the transport and activation of small molecules, and others.[1–11] Among them, potential tridentate N_2O donor Schiff bases are very popular for their mesmerizing ability to form both mononuclear facial and meridional isomers of bis-ligand complexes as well as varieties of poly-nuclear complexes by exploiting the bridging efficiency of their phenolate oxygen atoms along with many other type of complexes.[12–24] They have also been used as mono-/bi-dentate ligands for keeping other donor centers pendant.[25,26] Focusing on cobalt(III) complexes of N, O donor Schiff bases, many studies have been reported in the literature regarding their bio-mimetic catalytic activity, such as phenoxazinone synthase mimicking and catechol oxidase mimicking activity.[27–31] It is, however, true that cobalt has not been found in the active site structure of any metallo-oxidase yet, probably because of the inert character of cobalt(III), but this inert character of cobalt(III) attracts the interests of coordination chemists to synthesize bio-mimetic catalysts with cobalt(III), so that the intermediate species formed in the catalytic cycle could be identified easily and the mechanistic pathway of a catalytic reaction could be figured out.[29] The exploration of opto-electronic properties of cobalt(III) complexes of Schiff base ligands is also a growing research topic owing to the low cost and good availability of the metal sources and the structural flexibility and stability of the ligands.[32] The utilization of cobalt(III) complexes to model photosynthesis systems, where they have been used for either

[a]*Department of Chemistry, Inorganic Section, Jadavpur University, Kolkata 700032, India. E-mail: shouvik.chattopadhyay@jadavpuriuniversity.in; Tel: +91-33-24572941*
[b]*Department of Chemistry, Universitat de les Illes Balears, Crta de Valldemossa Km 7.5, 07122 Palma de Mallorca (Baleares), Spain. E-mail: toni.frontera@uib.es*
[c]*School of Chemistry, The University of Reading, P.O. Box 224, Whiteknights, Reading RG6 6AD, UK*

† Electronic supplementary information (ESI) available: Figures from S1 to S9 and details of Hirshfeld surface analysis. CCDC 2259434, 2259435 and 2259436 contain the supplementary crystallographic data for complexes **1**, **2**, and **3**, respectively. CCDC 2259434–2259436. For ESI and crystallographic data in CIF or other electronic format see DOI: **https://doi.org/10.1039/d3ra03828a**

the oxidation of water to O_2 or reduction of H^+ to H_2 or both, has also been reported in the literature.[33–38]

On the other hand, to construct an interesting supramolecular architecture by modulating various non-covalent interactions is an appealing research topic today.[39–41] A large number of supramolecular systems based on transition metal complexes have been used as probes, sensors, and photonic devices in last couple of years.[42–48] Several non-covalent intermolecular forces, such as hydrogen bonding, π–π stacking, cation-π, C–H···π interactions, halogen bonding, and ion pairing, have been used by crystal engineers to direct the pattern of numerous supramolecular assemblies.[49–64] An important role is also played by these non-covalent interactions in drug–receptor interactions, crystal engineering, enzyme inhibition, protein folding, *etc.*[65–69] The relevance of several non-covalent interactions has therefore been analyzed by means of theoretical and experimental investigations.[70,71]

In the present work, we synthesized three cobalt(III) complexes, namely $[Co^{III}(HL^1)_2(N_3)_2]ClO_4$ (**1**), $[Co^{III}(L^2)(HL^2)(N_3)]ClO_4\cdot 1.5H_2O$ (**2**), and $[Co^{III}(L^3)(HL^3)(NCS)]_2[Co^{II}Cl_2(NCS)_2]$ (**3**), with tridentate N_2O donor Schiff base ligands, namely HL^1 = 2-(3-(dimethylamino) propyliminomethyl)-6-methoxyphenol, HL^2 = 2-(2-(dimethylamino)ethyliminomethyl)-4,6-dichlorophenol, and HL^3 = 2-(2-(dimethylamino)ethyliminomethyl)-6-methoxyphenol. Both **1** and **2** are cationic complexes, whereas both cationic and anionic complexes are present in **3**. The CH···X contacts (X = C, N, S, Cl) make a strong contribution to the total Hirshfeld surface and have a predominant role in the crystal packing of complexes **1–3** (see Scheme 1). Complexes **1** and **2** form self-assembled dimers, where the azide co-ligands interact with several aliphatic CH bonds of the Schiff base ligand. In the case of **2**, additional CH···π interactions are also established that further stabilize the assemblies. Complex **3** forms a tetrameric assembly, where the $[CoCl_2(SCN)_2]^-$ anion is surrounded by three counter-cations and a network of CH···N,S,C interactions are established. The interaction energies were evaluated here using the quantum theory of atoms in molecules (QTAIM) and the potential energy density (Vr) predictor. This method is very useful as the interactions can be established between charged systems. Conventional procedures based on the supramolecular approach would lead to repulsive cation···cation interactions in **1** and **2** or to very large and attractive interactions for the anion···cation interactions in **3**. The evaluation of the CH···X (X = C, N, S, Cl) contacts using the QTAIM Vr predictor is also free from the effect of pure Coulombic forces.

Experimental section

Materials

All the starting materials and solvents were commercially available, reagent grade, and used as purchased from Sigma-Aldrich without further purification.

Synthesis of the ligands

Synthesis of 2-(3-(dimethylamino)propyliminomethyl)-6-methoxyphenol (HL^1). The Schiff base ligand HL^1 was prepared by refluxing *N*,*N*-dimethyl-1,3-diaminopropane (~1 mmol, 0.1 mL) with 3-methoxysalicylaldehyde (~1 mmol, 0.160 g) in methanol (20 mL) for *ca* 1 h. The ligand was not isolated and the methanol solution was used directly for the preparation of complex **1**.

Synthesis of 2-(2-(dimethylamino)ethyliminomethyl)-4,6-dichlorophenol (HL^2). The Schiff base ligand HL^2 was prepared by refluxing a methanol solution (20 mL) of *N*,*N*-dimethyl-1,2-diaminoethane (~1 mmol, 0.1 mL) with 3,5-dichlorosalicylaldehyde (~1 mmol, 0.190 g) in methanol (20 mL) for *ca* 1 h. The ligand was not isolated and the methanol solution was used directly for the preparation of complex **2**.

Synthesis of 2-(2-(dimethylamino)ethyliminomethyl)-6-methoxyphenol (HL^3). The Schiff base ligand HL^3 was synthesized in a similar method to that of HL^2, except that 3-methoxysalicylaldehyde (~1 mmol, 0.160 g) was used instead of 3,5-dichlorosalicylaldehyde. The ligand was not isolated and was used directly for the preparation of complex **3**.

Synthesis of the complexes

Synthesis of $[Co^{III}(HL^1)_2(N_3)_2]ClO_4$ (1). A methanol solution (5 mL) of cobalt(II) perchlorate hexahydrate (1 mmol, 0.365 g) was added to the methanol solution of the ligand HL^1, followed by the addition of a methanol solution (5 mL) of sodium azide (1 mmol, 0.065 g) with constant stirring. The stirring was continued for an additional 2 h. Dark brown diffraction quality single crystals were obtained after a few days slow evaporation of the solution in an open atmosphere.

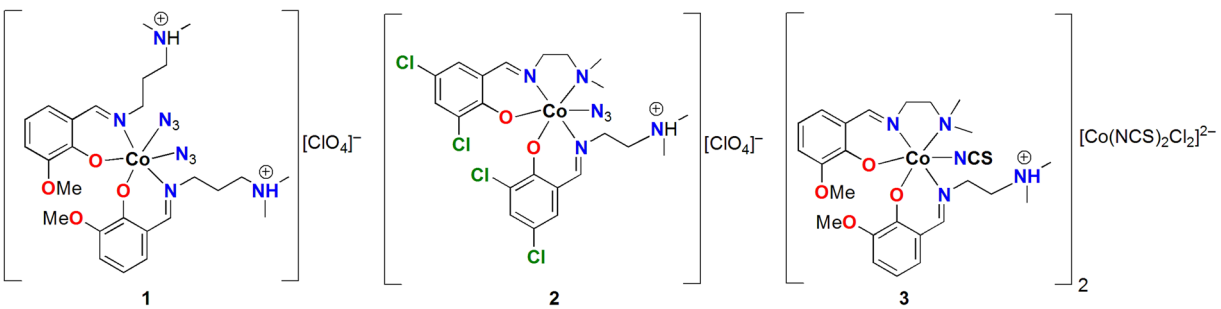

Scheme 1 Molecular diagrams complexes **1–3**.

Yield: 0.50 g {70%}. Anal. Calc. for $C_{26}H_{40}ClCoN_{10}O_8$ (FW 717.08): C, 43.55; H, 5.90; N, 19.53%; found: C, 43.53; H, 5.87; N, 19.54%. IR (KBr, cm^{-1}): 1623 ($\nu_{C=N}$), 2012, 2023 (ν_{N3}), 3232, 3293 (ν_{N-H}), 2968–2806 (ν_{CH}). UV-vis, λ_{max} (nm), [ε_{max} (L mol^{-1} cm^{-1})] (CH_3CN), 246 nm [5.1×10^4], 426 nm [5.06×10^3], 708 nm [1.69×10^3]. Magnetic moment: diamagnetic. ESI-MS (positive ion mode, CH_3CN) *m*/*z*: 529.06 $[Co(L^1)_2]^+$. ^{1}H NMR (DMSO-*d*6) (ppm) δ: 8.03 (s, 2H, benzylic CH), 6.90 (d, 4H, H atom, attached to the nitrogen of $^+NHMe_2$ group, and aromatic CH), 6.79 (dd, $J = 1.5$ Hz, 2H, aromatic CH), 6.43 (dd, $J = 7.5$ Hz, 2H, aromatic CH), 3.85–3.75 (m, 10H, $-OCH_3$ and $=N-CH_2$), 3.18–1.24 (m, 20H, methyl protons of $^+NHMe_2$ groups and methylene protons).

Synthesis of $[Co^{III}(L^2)(HL^2)(N_3)]ClO_4 \cdot 1.5H_2O$ (2). Complex **2** was prepared in a similar method to that of complex **1** except that HL^2 was used instead of HL^1. Diffraction quality dark brown single crystals were obtained after a few days slow evaporation of the solution in an open atmosphere.

Yield: 0.78 g {52%}. Anal. Calc. for $C_{44}H_{58}Cl_{10}Co_2N_{14}O_{15}$ (FW 1495.40): C, 35.34; H, 3.91; N, 13.11%; found: C, 35.33; H, 3.90; N, 13.13%. IR (KBr, cm^{-1}): 1637 ($\nu_{C=N}$), 2022 (ν_{N3}), 3292 (ν_{N-H}), 2968–2806 (ν_{CH}). UV-vis, λ_{max} (nm), [ε_{max} (L mol^{-1} cm^{-1})] (CH_3CN), 314 nm [1.40×10^4], 404 nm [6.7×10^3], 638 nm [1.21×10^2]. Magnetic moment: diamagnetic. ESI-MS (positive ion mode, CH_3CN) *m*/*z*: 578.81 $[Co(L^2)_2]^+$. ^{1}H NMR (DMSO-*d*6) (ppm) δ: 8.50 (s, 2H, benzylic CH), 7.47 (s, $J = 1.5$ Hz, 2H, aromatic CH), 7.40 (s, 3H, aromatic CH and H atom attached to N of $^+NHMe_2$ group), 3.18 (t, $J = 7.1$ Hz, 6H, methylene protons), 2.91–2.05 ($J = 7.1$ Hz, 8H, methylene protons and methyl protons of $^+NHMe_2$ group), 1.57–1.24 (s, 6H, methyl protons of NMe_2).

Synthesis of $[Co^{III}(L^3)(HL^3)(NCS)]_2$ $[Co^{II}Cl_2(NCS)_2]$ (3). A methanol solution (5 mL) of cobalt(II) chloride tetrahydrate (~3 mmol, 0.510 g) was then added to the methanol solution of the ligand HL^3, followed by the addition of a methanol solution (5 mL) of sodium thiocyanate (~4 mmol, 0.330 g) with constant stirring. The stirring was continued for an additional 2 h. Dark brown single crystals suitable for X-ray diffraction were obtained after a few days slow evaporation of the solution in an open atmosphere.

Yield: 0.75 g {55%}. Anal. Calc. for $C_{52}H_{70}Cl_2Co_3N_{12}O_8S_4$ (FW 1365.17): C, 45.68; H, 5.16; N, 12.29%; found: C, 45.66; H, 5.14; N, 12.30%. IR (KBr, cm^{-1}): 1647 ($\nu_{C=N}$), 2023, 2065 (ν_{NCS}), 2968–2806 (ν_{CH}). UV-vis, λ_{max} (nm), [ε_{max} (L mol^{-1} cm^{-1})] (CH_3CN), 388 nm [1.28×10^4], 572 nm [1.29×10^3], 654 nm [1.27×10^3]. Magnetic moment: $\mu = 3.78$ B.M. ESI-MS (positive ion mode, CH_3CN) *m*/*z*: 500.99 $[Co(L^3)_2]^+$, 501.99 $[Co(L^3)(HL^3)]^+$.

Physical measurements

Elemental analyses (carbon, hydrogen, and nitrogen) were performed using a PerkinElmer 240C elemental analyzer. IR spectra in KBr (4500–500 cm^{-1}) were recorded with a PerkinElmer RX-1 FTIR spectrophotometer. Electronic spectra in acetonitrile were recorded on a UV-vis spectrofluorometer, SHIMADZU (UV-1900i). The magnetic susceptibility measurements were done with an EG&PAR vibrating sample magnetometer, model 155, at room temperature, with diamagnetic corrections made using Pascal's constants. Effective magnetic moments were calculated using the formula $\mu_{eff} = 2.828(\chi_M T)^{1/2}$, where χ_M is the corrected molar susceptibility. Electrospray ionization mass spectra were recorded on a Waters Xevo G2 Q-TOF instrument. ^{1}H NMR spectra were recorded using a BRUKER 400 MHz NMR spectrometer in DMSO-*d*6 solvent, with MestReNova software used for plotting the NMR data.

Table 1 Crystal data and refinement details for complexes **1**, **2**, and **3**

Complex	**1**	**2**	**3**
Formula	$C_{26}H_{42}ClCoN_{10}O_8$	$C_{44}H_{58}Cl_{10}Co_2N_{14}O_{15}$	$C_{52}H_{70}Cl_2Co_3N_{12}O_8S_4$
Formula weight	717.08	1495.40	1367.13
Temperature (K)	273(2)	273(2)	273(2)
Crystal system	Orthorhombic	Triclinic	Triclinic
Space group	*Pbcn*	$P\bar{1}$	$P\bar{1}$
a (Å)	12.8143(7)	8.2780(6)	10.3465(4)
b (Å)	17.6436(10)	13.6175(9)	15.4956(6)
c (Å)	14.6798(9)	15.2737(10)	20.7242(9)
α	(90)	68.354(2)	105.535(1)
β	(90)	82.668(2)	101.074(1)
γ	(90)	86.839(2)	97.799(1)
Z	4	1	2
d_{calc} (g cm^{-3})	1.435	1.564	1.474
μ (mm^{-1})	0.659	1.015	1.081
F(000)	1504	764	1418
Total reflections	106 239	44 389	91 950
Unique reflections	2957	5680	10 987
Observed data [$I > 2\sigma(I)$]	2735	5065	9723
No. of parameters	231	399	762
R(int)	0.048	0.039	0.048
R_1, wR_2 (all data)	0.0752, 0.2322	0.0553, 0.1484	0.0527, 0.1143
R_1, wR_2 [$I > 2\sigma(I)$]	0.0716, 0.2265	0.0498, 0.1420	0.0465, 0.1099

Table 2 Selected bond lengths (Å) in the coordination of cobalt(III) in the cationic units of complexes 1, 2, and 3

			3	
Complex	1	2	(For Cation A)	(For Cation B)
Co(1)-N(1)	—	2.042(3)	2.037(3)	2.038(3)
Co(1)-N(2)	1.954(4)	1.895(3)	1.900(3)	1.898(2)
Co(1)-N(3)	1.967(4)	1.942(3)	1.927(3)	1.942(3)
Co(1)-N(4)	—	1.962(3)	1.951(3)	1.953(3)
Co(1)-O(1)	1.899(2)	1.888(3)	1.924(2)	1.908(2)
Co(1)-O(2)	—	1.910(2)	1.882(2)	1.881(2)

Table 3 Selected bond lengths (Å) in the coordination sphere of cobalt(II) in the anionic unit of complex 3

Co(2)-N(6)	1.977(4)
Co(2)-N(7)	2.034(5)
Co(2)-Cl(1)	2.2845(11)
Co(2)-Cl(2)	2.2600(15)

X-ray crystallography

Suitable single crystals of all three complexes were used for data collection using a 'Bruker D8 QUEST area detector' diffractometer equipped with graphite-monochromated Mo Kα radiation ($\lambda = 0.71073$ Å) at 110 K. The molecular structures were solved by direct methods and refined by full-matrix least squares on F^2, using the SHELX-18/1 package.[72] Anisotropic thermal parameters were used for the refinement of the non-hydrogen atoms. Hydrogen atoms attached to oxygen atoms were located by different Fourier maps and were kept at fixed positions. All other hydrogen atoms were placed in their geometrically idealized positions and constrained to ride on their parent atoms. Multi-scan empirical absorption corrections were applied to the data using the program SADABS.[73] A summary of the crystallographic data and refinement details of all three complexes are given in Table 1. Selected bond lengths are listed in Tables 2 and 3, while selected bond angles are listed in Tables 4 and 5.

Table 4 Selected bond angles (°) in the coordination of cobalt(III) in the cationic units of complexes 1, 2, and 3

			3	
Complex[a]	1	2	(For cation A)	(For cation B)
N(1)-Co(1)-N(2)	—	85.15(13)	85.22(12)	86.21(12)
N(1)-Co(1)-N(3)	—	88.72(13)	90.43(12)	92.34(12)
N(1)-Co(1)-N(4)	—	94.76(11)	92.77(12)	93.64(12)
N(2)-Co(1)-N(2*)	178.96(13)	—	—	—
N(2)-Co(1)-N(3*)	87.53(17)	—	—	—
N(2)-Co(1)-N(3)	93.21(17)	89.90(12)	86.20(13)	84.40(12)
N(2)-Co(1)-N(4)	—	177.86(12)	177.19(11)	178.00(11)
N(3)-Co(1)-N(3*)	90.46(17)	—	—	—
N(3)-Co(1)-N(4)	—	92.24(12)	95.80(12)	97.60(12)
O(1)-Co(1)-O(1*)	90.05(10)	—	—	—
O(1)-Co(1)-O(2)	—	89.37(11)	88.90(9)	90.91(9)
O(1)-Co(1)-N(1)	—	178.27(11)	178.23(11)	177.77(11)
O(1)-Co(1)-N(2)	92.25(12)	94.91(12)	95.53(10)	95.94(10)
O(1)-Co(1)-N(2*)	87.01(12)	—	—	—
O(1)-Co(1)-N(3)	174.54(16)	89.56(12)	88.03(11)	88.48(11)
O(1)-Co(1)-N(3*)	90.01(14)	—	—	—
O(1)-Co(1)-N(4)	—	85.25(11)	86.53(10)	84.20(10)
O(2)-Co(1)-N(1)	—	92.35(11)	92.78(11)	88.74(11)
O(2)-Co(1)-N(2)	—	84.03(12)	83.44(11)	83.37(10)
O(2)-Co(1)-N(3)	—	173.73(12)	168.85(11)	167.62(11)
O(2)-Co(1)-N(4)	—	93.83(11)	94.71(10)	94.64(10)

[a] Symmetry transformation* = $1 - x, y, 3/2 - z$.

Table 5 Selected bond angles (°) in the coordination sphere of cobalt(II) in the anionic unit of complex 3

N(6)-Co(2)-N(7)	104.62(18)
Cl(1)-Co(2)-Cl(2)	110.84(5)
Cl(1)-Co(2)-N(6)	109.16(12)
Cl(1)-Co(2)-N(7)	107.90(12)
Cl(2)-Co(2)-N(6)	111.21(14)
Cl(2)-Co(2)-N(7)	112.85(14)

Hirshfeld surface analysis

Hirshfeld surfaces[74–76] and the associated two-dimensional (2D) fingerprint[77–79] plots were calculated using Crystal Explorer,[80] with bond lengths to hydrogen atoms set to the standard values.[81] The Hirshfeld surface is unique for a fixed CIF.[82]

Theoretical methods

The calculations reported in this manuscript were performed using the Turbomole 7.2 program[83] and the BP86-D3/def2-TZVP level of theory.[84,85] The X-ray geometries were used instead of fully optimized geometries because we wanted to evaluate the CH···C,N,S,Cl as they stand in the solid state. The NCI plot[86] reduced density gradient (RGD) isosurfaces were used to characterize the non-covalent interactions since combining both methods can reveal more about the non-covalent interactions in real space. The cubes needed to generate the NCI plot surfaces were computed at the same level of theory using the wave functions generated by means of the Turbomole 7.2 program. The NCI plot index isosurfaces corresponded to both favorable and unfavorable interactions, as differentiated by the sign of the second density Hessian eigenvalue and defined by the isosurface color. The QTAIM analysis[87] and the cube files from the wave functions were computed at the same level of theory by means of the MULTIWFN program[88] and represented using VMD software.[89]

Results and discussion

Synthesis

3-Methoxysalicylaldehyde was refluxed in methanol with *N*,*N*-dimethyl-1,3-diaminopropane to form compartmental Schiff base ligand, HL^1, following the literature method.[90–92] This Schiff base upon reaction with cobalt(II) perchlorate hexahydrate and sodium azide produced the mononuclear complex, **1**. The formation process of this complex is shown in Scheme 2.

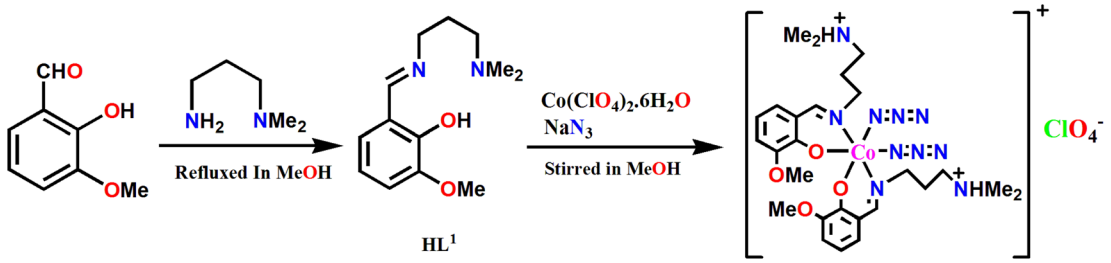

Scheme 2 Synthetic route to complex 1.

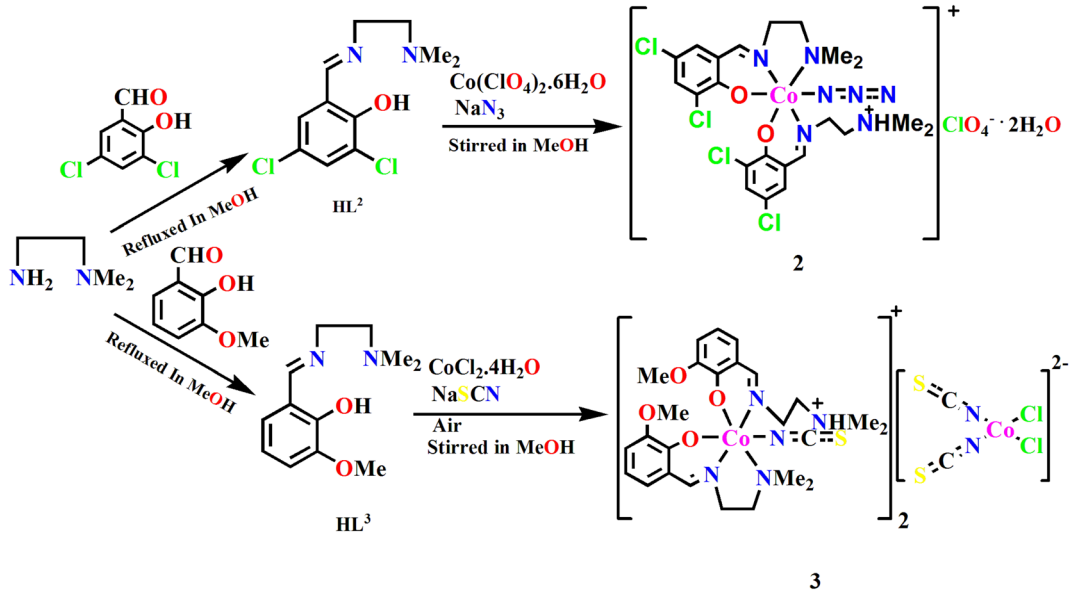

Scheme 3 Synthetic routes to complexes 2 and 3.

On the other hand, 3,5-dichlorosalicylaldehyde and 3-methoxysalicylaldehyde were refluxed in methanol with *N*,*N*-dimethyl-1,2-diaminoethane to form the compartmental Schiff base ligands HL^2 and HL^3 respectively following the literature method. HL^2 upon reaction with cobalt(II) perchlorate hexahydrate and azide gave mononuclear complex **2**. Similarly, HL^3 upon reaction with cobalt(II) chloride tetrahydrate and sodium thiocyanate gave mononuclear complex **3**. Here, cobalt(II) was first oxidized to cobalt(III) by areal oxygen in the presence of the Schiff base ligand producing a strong crystal field, as has also been observed in similar complexes.[27,93,94] The formation of the complexes is shown in Scheme 3.

Description of the structures

$[Co^{III}(HL^1)_2(N_3)_2]ClO_4$ (1). Complex **1** crystallizes in the orthorhombic space group, *Pbcn*. A perspective view of complex **1** with the selective atom numbering scheme is shown in Fig. 1. The structure of the complex consists of a hexa-coordinated cobalt(III) in a distorted octahedral geometry. A non-coordinated perchlorate is also present. The Schiff base ligand (HL^1) is trapped in its zwitterionic form. The cobalt(III) center is coordinated by two imine nitrogen atoms, N(2) and N(2)*, and two phenolate oxygen atoms, O(1) and O(1)*, of the Schiff base (where, the symmetry transformation* = $1-x$, y, $3/2-z$). The fifth and sixth coordination sites of cobalt(III) are occupied by two nitrogen atom, N(3) and N(3)*, of two terminal azides to complete its octahedral geometry. The azides occupy *cis* positions. Each azide is quasi-linear with the N–N–N angle being 170.1(6)°, as expected.[27,95] The bond lengths and bond angles of the complex are comparable with previously reported octahedral cobalt(III) Schiff base complexes.[92,95]

The hydrogen atoms, H(3B), attached to the carbon atom C(3), and H(4A), attached to the carbon atom, C(4), of one molecule are involved in intermolecular hydrogen bonding interactions, with the azide nitrogen atoms N(4A)^a and N(5A)^a, respectively, {symmetry transformation, $a = 1-x, 1-y, 1-z$} of a neighboring molecule, thus forming a self-assembled dimer (Fig. 2). The details of these interactions are listed in Table 6.

$[Co^{III}(L^2)(HL^2)(N_3)]ClO_4 \cdot 1.5H_2O$ (2). Complex **2** crystallizes in the triclinic space group, $P\bar{1}$. A perspective view of complex **2** with the selective atom numbering scheme is shown in Fig. 3. The structure of the complex consists of a hexa-coordinated cobalt(III) in a distorted octahedral geometry. One molecule of the Schiff base ligand (HL^1) is trapped in its zwitterionic form, while the other is trapped in its anionic form. The cobalt(III)

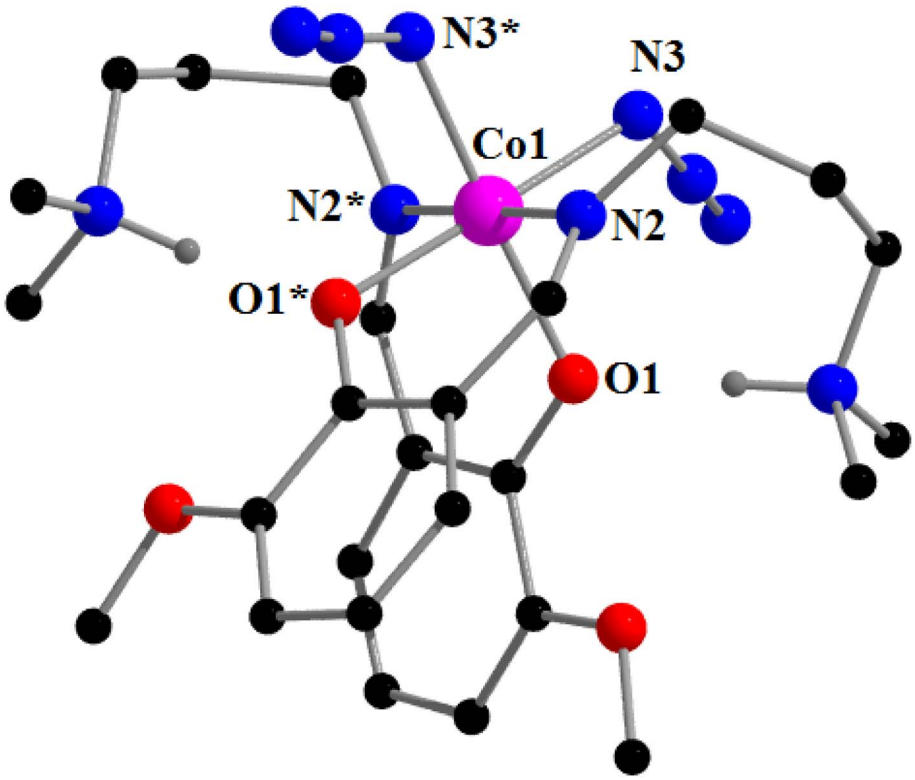

Fig. 1 Perspective view of complex **1** with the selective atom numbering scheme. Perchlorate anion is not shown for clarity. Only two hydrogen atoms (attached with two amine nitrogen atoms) are shown. Symmetry transformation* = $1 - x, y, 3/2 - z$.

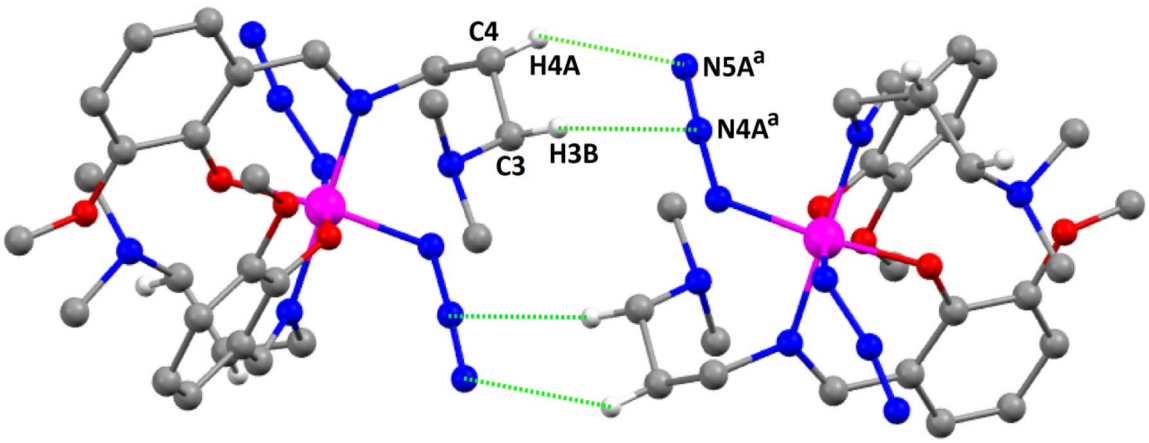

Fig. 2 Perspective view of the hydrogen bonding interactions in complex **1**. Only the relevant hydrogen atoms are shown for clarity. Symmetry transformation, $a = 1 - x, 1 - y, 1 - z$.

center in this complex is meridionally coordinated by one amine nitrogen atom, N(1), one imine nitrogen atom, N(2), and one phenolate oxygen atom, O(1) of a deprotonated Schiff base, and one imine nitrogen atom, N(4), and one phenolate oxygen atom, O(2), of the zwitterionic Schiff base. An azide nitrogen atom, N(3), occupies the sixth coordination site of cobalt(III) to complete its distorted octahedral geometry. The cobalt(III)–N_{imine} distance {1.895(3) Å} is shorter than the cobalt(III)–N_{amine} distance {2.043(3) Å}, as has also been observed in similar systems[90,92,96,97] The terminal azide is quasi-linear with the N–N–N angle being 175.9 (4)°, as expected.[27,95] The saturated five membered chelate ring, Co(1)-N(1)-C(3)-C(4)-N(2), represents a half chair conformation (Fig. 4) with puckering parameters[98] $Q = 0.407(4)$ Å, $\varphi(2) = 61.4(5)°$.

The hydrogen atom, H(12C), attached with the carbon atom, C(12), is involved in intermolecular CH···N with the azide nitrogen atom, $N(7)^b$, of a symmetry related {symmetry transformation, $b = 1 - x, 1 - y, -z$} neighboring molecule, also

Table 6 List of non-covalent interactions studied in the complexes[a]

Complex	Atoms involved (D–H···A)	Interaction	Distance D–H (Å)	Distance H···A (Å)	Distance D···A (Å)	Angle D–H···A (°)
1	C(3)-H(3B)···N(4A)[a]	CH···N	0.971(4)	3.081(5)	3.568(7)	145.7(3)
	C(4)-H(4A)···N(5A)[a]	CH···N	0.969(5)	2.693(7)	3.537(8)	112.6(3)
2	C(12)-H(12C)···N(7)[b]	CH···N	0.960(5)	2.587(4)	3.489(6)	156.7(3)
	C(13)-H(13B)···Cg(1)[b]	CH···π	0.960(7)	3.321	3.694	105.44
3	C(2)-H(2A2)···S(3)	CH···S	0.960(4)	2.956(1)	3.602(4)	125.7(3)
	C(2)-H(2A3)[c]···S(2)	CH···S	0.960(3)	2.972(1)	3.915(3)	167.6(3)
	C(3)-H(3A2)[c]···Cl(1)	CH···Cl	0.970(5)	2.871(1)	3.742(5)	149.8(2)
	C(15)-H(15A)···Cl(1)	CH···Cl	0.970(5)	2.737(1)	3.649(5)	156.8(3)
	C(17)-H(17A)···Cl(1)	CH···Cl	0.930(3)	2.867(1)	3.734(3)	155.7(2)
	C(13)-H(13D)···S(3)	CH···S	0.960(1)	3.032(2)	3.93(1)	157.4(6)
	C(14)-H(14F)···S(2)	CH···S	0.960(1)	2.888(1)	3.65(1)	136.8(7)

[a] Symmetry transformation, $a = 1-x, 1-y, 1-z$; $b = 1-x, 1-y, -z$ and $c = 1+x, y, z$. Cg(1)[b] is the centroid of the aromatic ring, R(1)[b] [C(6)[b]-C(7)b-C(8)[b]-C(9)[b]-C(10)[b]-C(11)[b]].

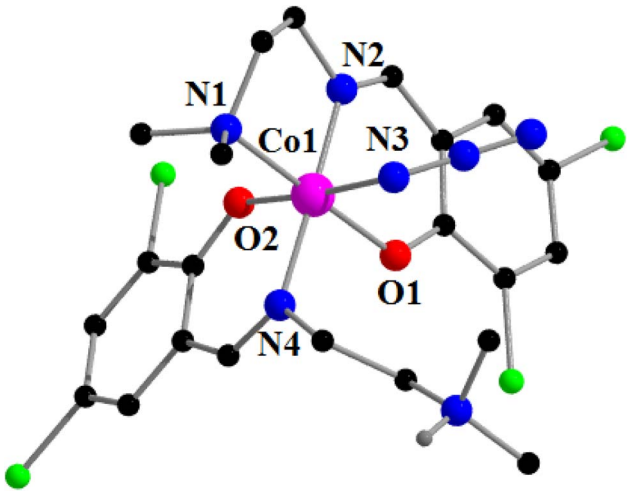

Fig. 3 Perspective view of complex **2** with the selective atom numbering scheme. Perchlorate anion and lattice water molecules are not shown for clarity. Only one hydrogen atom (attached with the amine nitrogen atom) is shown.

forming a self-assembled dimer. This dimer is further stabilized by CH···π interactions between the hydrogen atom, H(13A), attached to the carbon atom, C(13), and the centroid, Cg(1)[b], of the aromatic ring, R(1)[b] [C(6)[b]-C(7)[b]-C(8)[b]-C(9)[b]-C(10)[b]-C(11)[b]].

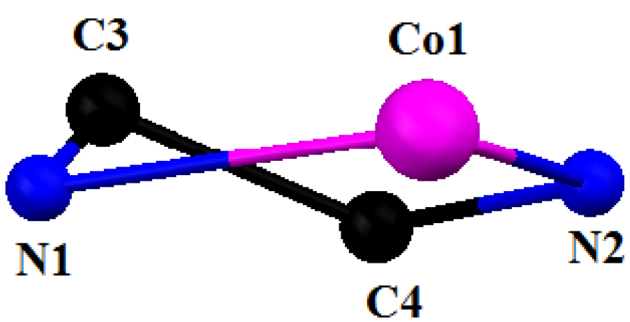

Fig. 4 Half chair conformation of complex **2** with the selective atom numbering scheme.

The dimer is shown in Fig. 5. The relevant CH···N and CH···π interactions observed in complex **2** are listed in Table 6.

$[Co^{III}(L^3)(HL^3)(NCS)]_2$ $[Co^{II}Cl_2(NCS)_2]$ (3). Complex **3** crystallizes in the triclinic space group, $P\bar{1}$. The asymmetric unit contains two crystallographically independent cationic units with the identical chemical formula $[Co^{III}(L_3)(HL^3)(NCS)]^+$ (may be designated as unit A and unit B) and one anionic unit, $[Co^{II}Cl_2(NCS)_2]$. A perspective view of one cationic unit (unit A) with the selective atom numbering scheme is shown in Fig. 5. The other cationic unit (unit B) has a more or less similar structure as that of unit A (Fig. S1 in the ESI†). A perspective view of the anionic unit of complex **3** is shown in Fig. 6. The structures of both the cationic and anionic units are described below.

The cobalt(III) centers are more or less octahedral in both cationic units (unit A or unit B), being bonded by one amine nitrogen atom, N(1), one imine nitrogen atom, N(2), and one phenolate oxygen atom, O(1), of the deprotonated Schiff base in a meridional fashion, one imine nitrogen atom, N(4), and one phenolate oxygen atom, O(2), of the zwitterionic Schiff base, and one thiocyanate nitrogen atom, N(3). The cobalt(III)–N_{imine} distances are shorter than the cobalt(III)–N_{amine} distances in both units, as has also been observed in similar systems.[96,97] In each cationic unit, the thiocyanate is almost linear, as evident from the N–C–S angle {179.1(3)° in unit A and 178.7(4)° in unit B}, as has also been observed in related systems.[27,99] The saturated five membered chelate rings, Co(1)-N(1)-C(3)-C(4)-N(2), represent envelope conformations with the puckering parameters[98] $Q = 0.427(4)$ Å, $\varphi(2) = 79.0(4)°$ for unit A and $Q = 0.427(4)$ Å, $\varphi(2) = 254.3(4)°$ for unit B. Fig. 7 shows the envelope configuration of the ring in unit A.

The anionic part of the complex consists of a tetra-coordinated distorted tetrahedral cobalt(II), being coordinated by two thiocyanate nitrogen atoms, N(6) and N(7), and two chloride ions, Cl(1) and Cl(2) (Fig. 8). The thiocyanates are quasi-linear with the N–C–S angles being 178.0 (4) ° and 177.6 (6)°, as expected.[100]

The thiocyanate sulfur atom, S(3), of the anionic unit forms bifurcated intermolecular hydrogen bonds with the hydrogen atoms H(2A2) {attached to carbon atom C(2)} of the cationic

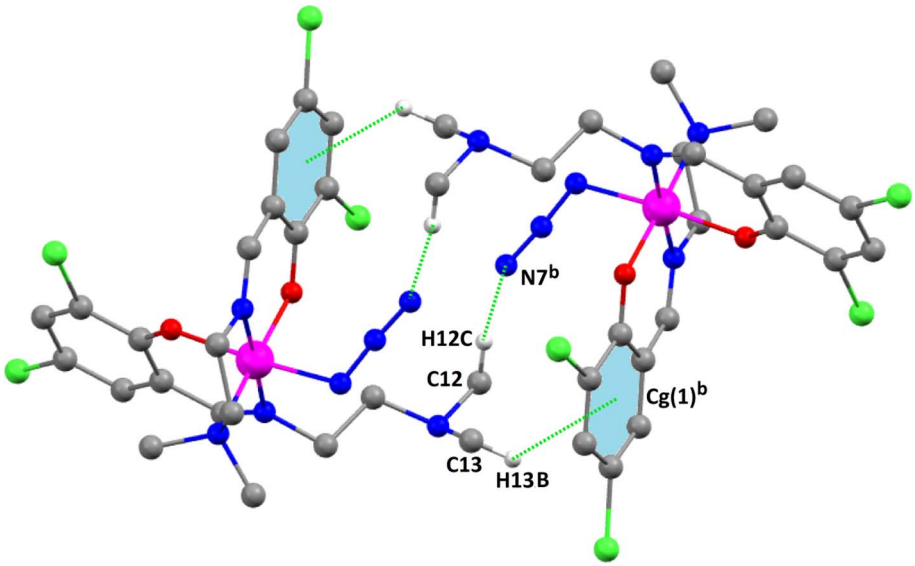

Fig. 5 Perspective view of the hydrogen bonding interactions in complex **2**. Only the relevant hydrogen atoms are shown for clarity. Symmetry transformation, ^{b} ($b = 1 - x, 1 - y, -z$).

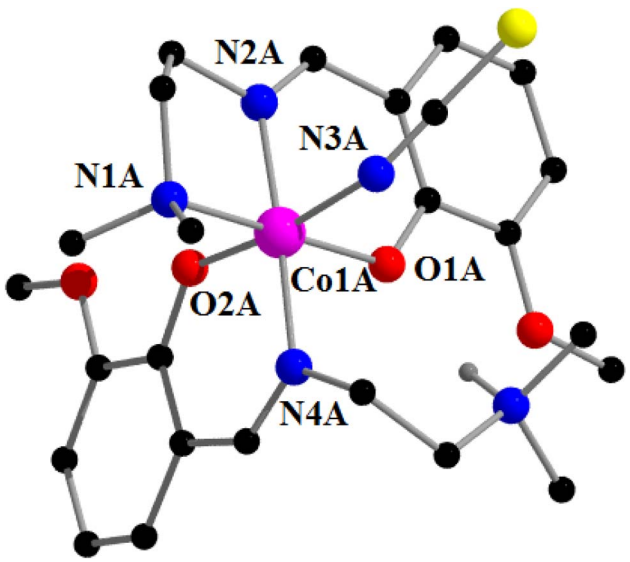

Fig. 6 Perspective view of the cationic part (unit A) of complex **3** with the selective atom numbering scheme. Only one hydrogen atom (attached with the amine nitrogen atom) is shown.

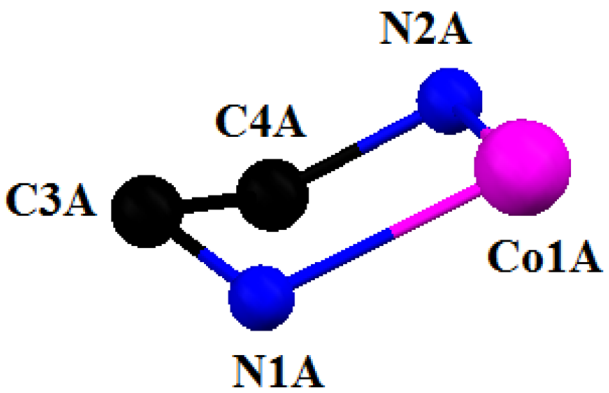

Fig. 7 Envelope conformation of the cationic part (unit A) of complex **3** with the selective atom numbering scheme.

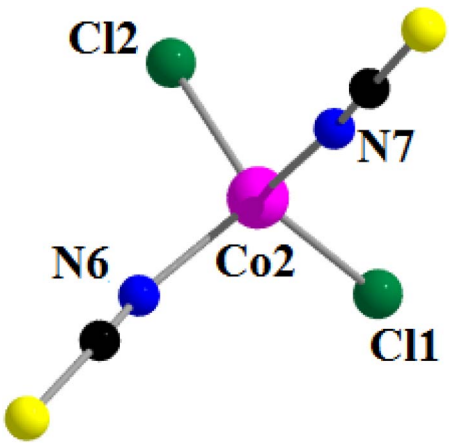

Fig. 8 Perspective view of the anionic part of complex **3** with the selective atom numbering scheme.

unit A and H(13D) {attached to carbon atom C(13)} of the cationic unit B. Another thiocyanate sulfur atom, S(2), of the anionic $[Co^{II}Cl_2(NCS)_2]^{2-}$ unit is also involved in intermolecular bifurcated hydrogen bonds with the hydrogen atoms, H(2A3)^{c} {attached to carbon atom C(2)^{c}} {Symmetry transformation, $c = 1 + x, y, z$}, of a neighboring cationic unit A and H(14F) {attached to carbon atom C(14)} of the cationic unit B, forming a 3D tetrameric assembly. The chlorine atom, Cl(1), of the anionic unit is involved in trifurcated hydrogen bonding with the hydrogen atoms H(15A), attached to C(15), H(17A), attached to C(17), and H(3A2)^{c}, attached to C(3)^{c} to further stabilize the

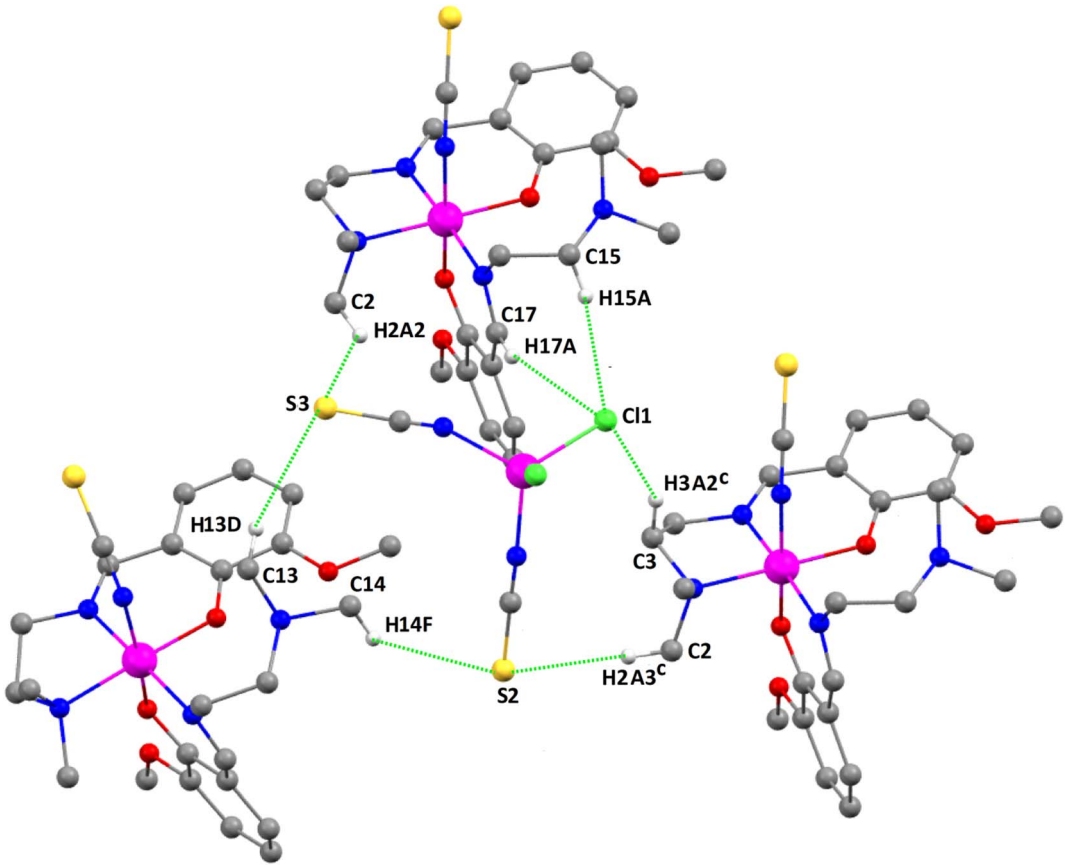

Fig. 9 Perspective view of the tetrameric assembly of complex **3**. Only the relevant hydrogen atoms are shown for clarity. Symmetry transformation, ^{c} (c = 1 + *x*, *y*, *z*).

tetrameric H-bonded assembly {Symmetry transformation, $c = 1 + x, y, z$} of the two cationic subunits A, as shown in Fig. 9.

Hirshfeld surface analysis

The Hirshfeld surfaces of all three complexes were mapped over d_{norm} (range ~0.1 Å to 1.5 Å), shape index, and curvedness (Fig. S6, ESI†). Red spots on the Hirshfeld surfaces denote the dominant interactions. The intermolecular interactions appear as distinct spikes in the 2D fingerprint plot showing the different spikes with their corresponding interactions. The dominant interactions in complex **1** corresponded to C···H/H···C (9.6%), O···H/H···O (21.1%), and N···H/H···N (24.4%) contacts. The proportion of C···H/H···C, O···H/H···O, N···H/H···N, and Cl···H/H···Cl interactions in complex **2** comprised 15.4%, 17.1%, 8.2%, and 31.7% of the Hirshfeld surface, respectively. Again the interactions in complex **3** comprised 16.2%, 10.2%, 17.2%, 6.6%, and 2.7% of the Hirshfeld surface as shown by the proportion of C···H/H···C, Cl···H/H···Cl, S···H/H···S, O···H/H···O, and N···H/H···N respectively. The 2D fingerprint plots of complexes **1**, **2**, and **3** are shown in Fig. 10–12, respectively.

Theoretical study on the supramolecular interaction

As commented in the previous section, the CH···X contacts (X = C, N, S, Cl) make a strong contribution to the total Hirshfeld surface and have a predominant role in the X-ray packing of complexes **1–3** (see Fig. 2, 5 and 9). In the case of complex **2**, additional CH···π interactions are established that further stabilize the assemblies. The CH···N distances range from 2.55 to 3.06 Å.

Fig. 9 shows a tetrameric assembly of complex **3**, where the $[CoCl_2(SCN)_2]^-$ anion is surrounded by three counter-cations, where a network of CH···N,S,C interactions are established with distances ranging from 2.74 to 3.03 Å. These long distances (also observed in the self-assembled dimers of **1** and **2**), along with the modest ability of C–H groups as H-bond donors, anticipate that each individual contact is weak. However, an additive number of contacts can lead to a significant stabilization of the system. This is the main purpose of the present theoretical study. The interaction energies were evaluated using the quantum theory of atoms in molecules and the potential energy density predictor. This method is very useful in systems like these reported herein where the interactions are established between charged systems. Conventional procedures based on the supramolecular approach would lead to repulsive cation···cation interactions in complexes **1** and **2** or to very large and attractive interactions for the anion···cation interactions in complex **3**. The evaluation of the CH···X (X = C, N, S, Cl) contacts using the QTAIM Vr predictor is free from the effect of pure Coulombic forces.

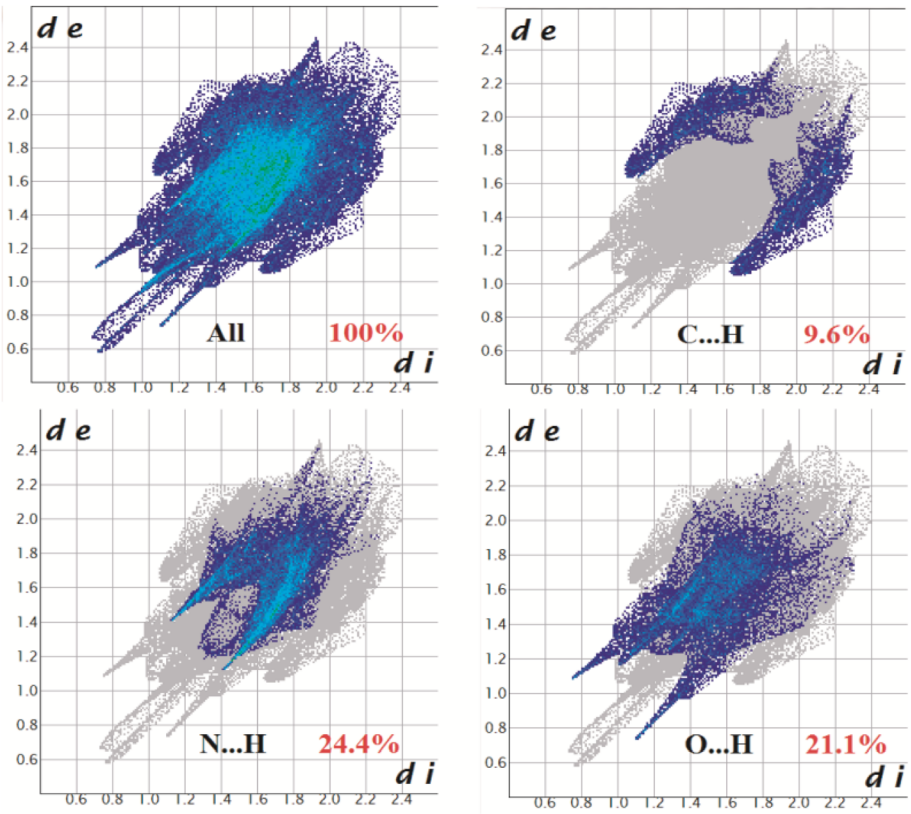

Fig. 10 Fingerprint plot of complex **1**: Full and resolved into C···H/H···C, N···H/H···N, and O···H/H···O contacts contributing to the total Hirshfeld surface area.

Fig. 13 shows the combined QTAIM/NCI plot characterization of the self-assembled dimers of complexes **1** and **2**. Each H-bond is characterized by a bond critical point (CP, red sphere) and bond path (orange line) connecting the H atom to the N atom. Moreover, a green RDG isosurface also appears upon dimerization, coincident with the location of the bond CPs. The

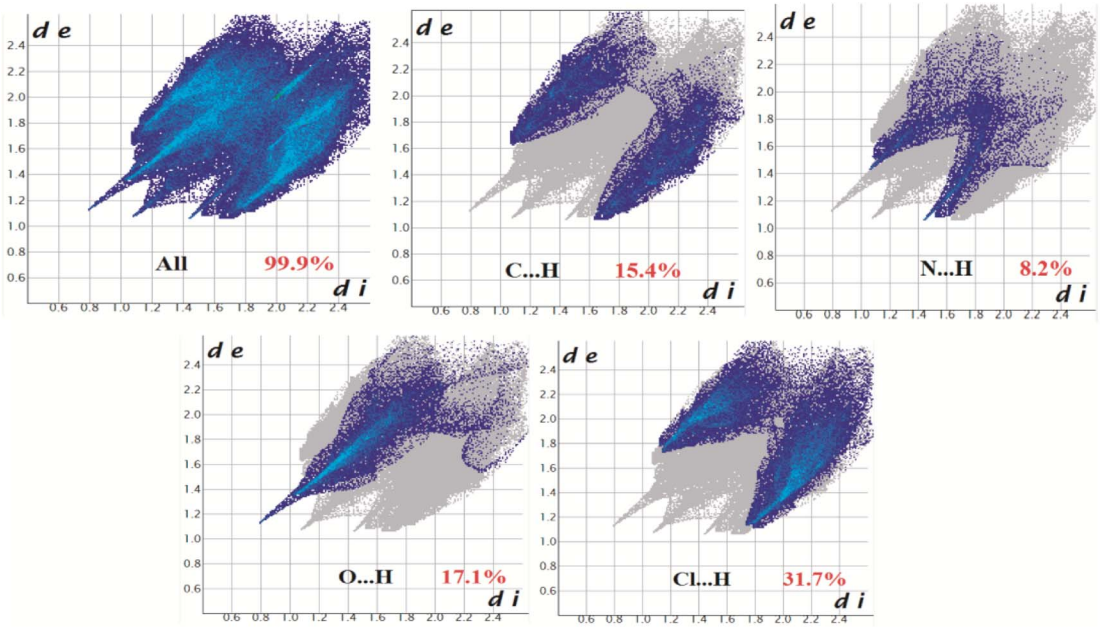

Fig. 11 Fingerprint plot of complex **2**: Full and resolved into C···H/H···C, N···H/H···N, O···H/H···O, and Cl···H/H···Cl contacts contributing to the total Hirshfeld surface area.

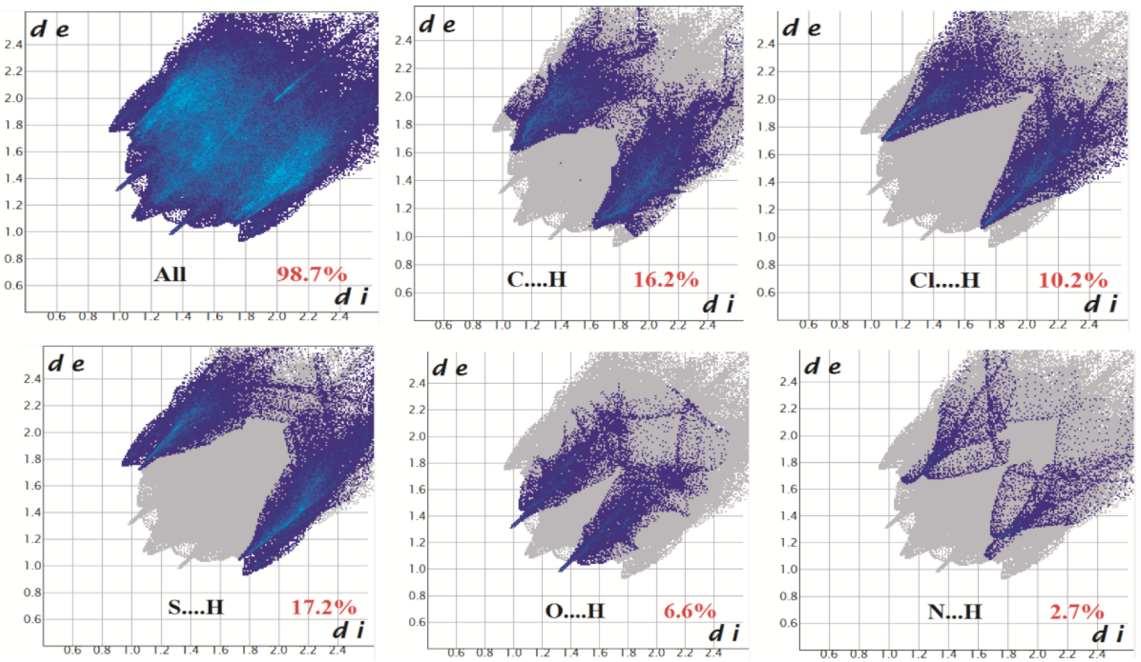

Fig. 12 Fingerprint plot of complex **3**: Full and resolved into C···H/H···C, Cl···H/H···Cl S···H/H···S, O···H/H···O, and N···H/H···N contacts contributing to the total Hirshfeld surface area.

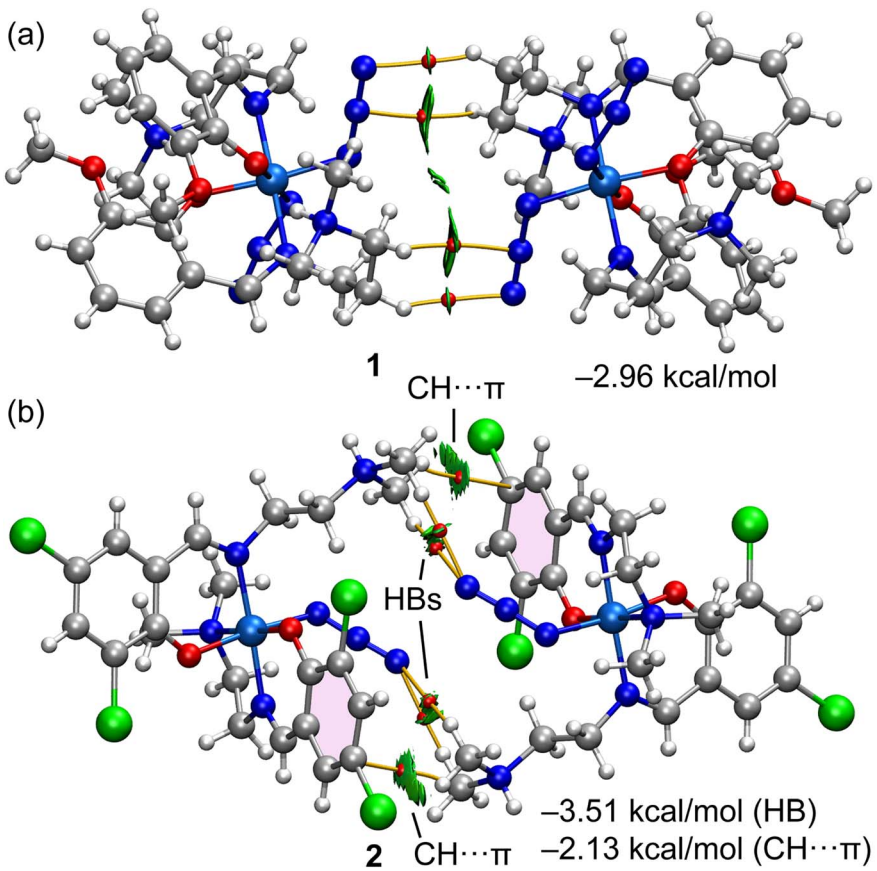

Fig. 13 QTAIM (bond CPs in red and bond path as orange lines) and NCI plot (RDG = 0.5, $\rho_{cut\text{-}off}$ = 0.04 a.u., color scale −0.035 a.u. ≤ (signλ_2)ρ ≤ 0.035 a.u.) for the self-assembled dimers of complexes **1** (a) and **2** (b). The interaction energies calculated using the Vr energy predictor are indicated in the figure. Only intermolecular interactions are represented.

green color of the isosurface reveals the CH···N contacts are weakly attractive. In the case of the dimer of complex **2**, the QTAIM/NCI plot analysis also confirmed the existence of the two symmetrically equivalent CH···π interactions, characterized by a bond CP, bond path, and extended green RDG isosurface that connects the CH bond to one C-atom of the aromatic ring. The interaction energy of the four H-bonds corresponding to the dimer of complex **1** is −2.96 kcal mol^{-1}, thus confirming the weak nature of each individual contact. The H-bond contribution in the dimer of complex **2** is similar (−3.51 kcal mol^{-1}) to the dimerization energy of complex **1**. The dimer is further reinforced with the CH···π interactions, which are slightly weaker (−2.13 kcal mol^{-1}) than the H-bonds.

Finally, Fig. 14 shows the combined QTAIM/NCI plot analysis of three heterodimers (ion pairs) extracted from the tetrameric assembly represented in Fig. 9. In the case of the dimer denoted as "A", the cationic part interacts with both SCN arms of the anion. The QTAIM/NCI plot analysis revealed a total of five CH···S contacts with an interaction energy of −3.29 kcal mol^{-1}, in line with the H-bonding energies of the self-assembled dimers. In the dimer denoted as "B" (Fig. 14b), the cationic part interacts with one Cl and one SCN ligand of the anionic counterpart. A total of three CH···Cl, two CH···N, and two CH···S contacts were revealed by the QTAIM/NCI plot analysis. The total interaction energy for this binding mode is moderately strong (−6.19 kcal mol^{-1}) due to this intricate network of H-bonds, confirming its importance in the solid-state architecture of complex **3**. The third dimer analyzed, denoted as "C" in Fig. 14c, presented a total of five contacts with a total interaction energy of −3.53 kcal mol^{-1}, similar to heterodimer "A" and those of complexes **1** and **2**.

The significant contribution of the CH···X (X = S, Cl, N) in complexes **1–3** agreed well with the Hirshfeld surface analysis since these type of contacts comprise most of the HS surface.

As previously indicated, the significance of CH···X contacts in the solid-state structures of complexes **1–3** was established without considering potent electrostatic influences. In order to comprehensively account for the role of Coulombic forces in stabilizing these complexes, we employed energy decomposition analysis for complexes **1** and **2** utilizing the Kitaura–Morokuma methodology.[101]

We assessed the relative contributions of the electrostatic, dispersion, orbital, and correlation terms to the stability of complexes **1** and **2**. Our findings, as illustrated in Fig. 15, underscore the paramount importance of the electrostatic term (depicted by blue bars), accounting for substantial stabilization energies of −44.70 kcal mol^{-1} and −45.53 kcal mol^{-1} for complexes **1** and **2**, respectively. Minor disparities are apparent in the exchange repulsion (depicted in red bars), dispersion (illustrated in green bars), and correlation (represented by violet bars) components, exhibiting resemblances across both complexes. Notably, a pronounced discrepancy of the surfaces in the orbital contribution was noted, significantly more pronounced in complex **1** than in complex **2**. Consequently, this

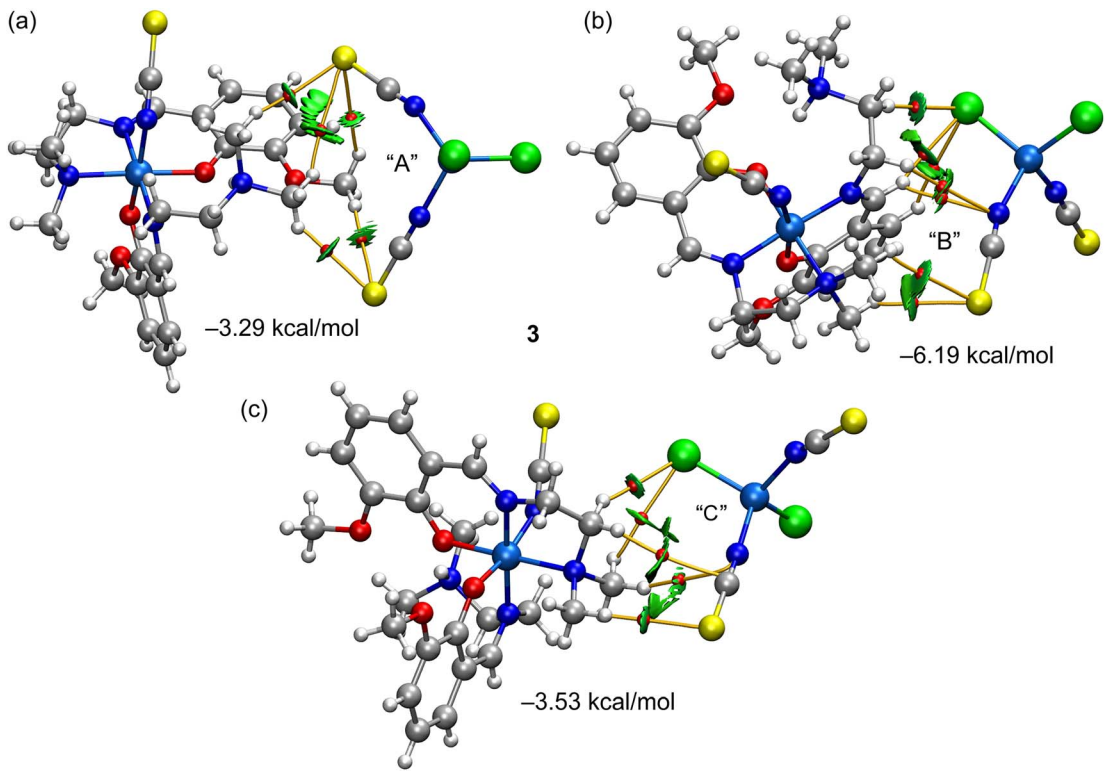

Fig. 14 (a–c) QTAIM (bond CPs in red and bond path as orange lines) and NCI plot (RDG = 0.5, $\rho_{cut\text{-}off}$ = 0.04 a.u., color scale −0.035 a.u. ≤ (signλ_2)ρ ≤ 0.035 a.u.) for the three dimers of complex **3**. The interaction energies calculated using the Vr energy predictor are indicated in the figure. Only intermolecular interactions are represented.

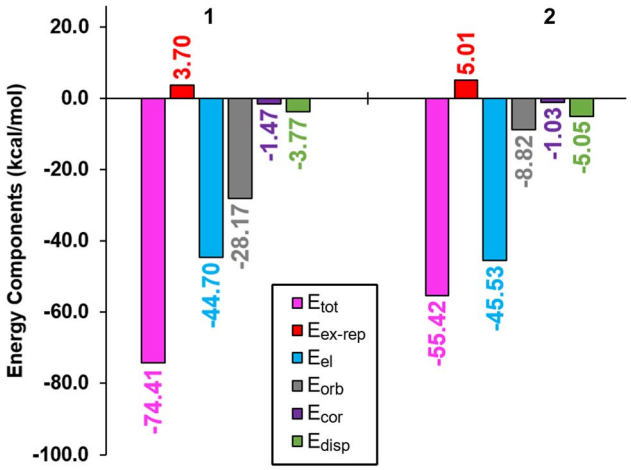

Fig. 15 Representation of the total (E_{tot}, pink), exchange repulsion ($E_{ex\text{-}rep}$, red), electrostatic (E_{el}, blue), orbital (E_{orb}, gray), correlation (E_{cor}, violet), and dispersion (E_{disp}, green) terms for the ion-pair complexes **1** (left) and **2** (right).

disparity yielded a notably higher total stabilization energy (portrayed in pink bars) in complex **1**. This variance likely stems from the closer proximity of the perchlorate anion to the Schiff base cation in complex **1**, culminating in shorter CH···O interactions (with the shortest CH···O distance measuring 2.24 Å in complex **1**, in contrast to 2.46 Å in complex **2**). It is well-established that orbital effects are acutely sensitive to distance, with larger distances resulting in diminished orbital overlap. This interpretation finds further support in the Hirshfeld surface analysis, where the CH···O contribution was registered at a higher 21.1% in complex **1** compared to 17.1% in complex **2**.

IR, electronic spectroscopy, ESI-MS, and ^{1}H-NMR studies

In the IR spectra of all three complexes, distinct bands due to azomethine (C=N) stretching vibrations appeared in the region of 1623–1647 cm^{-1}.[102–105] The sharp absorption bands located at 2015 and 2023 cm^{-1} (in **1**) and 2022 cm^{-1} (in **2**) indicated the presence of terminal azide (for **1** and **2**), while those at 2023 and 2065 cm^{-1} (in **3**) indicated the presence of N-bonded thiocyanate (for **3**),[106,107] respectively, which are also evident from crystal structure determination. The sharp bands at 3293 and 3232 cm^{-1} indicated N–H stretching vibrations in the IR spectrum of complex **1** and the sharp bands at 3292 cm^{-1} also indicated N–H stretching vibrations in the IR spectrum of complex **2** as well.[108–110] The characteristic absorption band for non-coordinated perchlorate anion appeared at 1076 cm^{-1} in the IR spectra of complexes **1** and **2**. The bands in the range of 3006–2806 cm^{-1} were due to alkyl C–H bond stretching vibrations, as customarily noticed in the IR spectra of all three complexes.[94,111] The IR spectra of all the complexes are given in Fig. S2–S4 (ESI).† These assignments were in good agreement with the theoretical calculations, as detailed in Table 7.

Electronic spectra of the complexes were recorded in acetonitrile medium at room temperature in the range of 200–800 nm. In the high-energy region, complex **1** showed intense absorption bands around 243–275 nm, corresponding to π–π* transitions.[28,112,113] Broad absorption bands at 314 nm (for **2**) and 388 nm (for **3**) were also observed, which were consistent with the LMCT band.[114–116] The electronic absorption spectra of all three complexes in acetonitrile medium showed d–d transition bands around 426 nm (for **1**), 404 nm (for **2**), and 654 nm (for **3**), as expected for a low spin cobalt(III) complex in an octahedral geometry.[117,118] The weak band around 708 nm (for **1**), 638 nm (for **2**), and 572 nm (for **3**) may be assigned as one of the two expected transitions for any low spin cobalt(III) complex in an octahedral geometry ($^1A_{1g} \rightarrow {}^1T_{1g}$ and $^1A_{1g} \rightarrow {}^1T_{2g}$). The UV spectrum of complex **3** is given in Fig. S5 (ESI).†

The molecular ion peaks in acetonitrile solution appeared at m/z = 529.0591 for complex **1** (theoretical m/z = 529.55 for $[Co(L^1)_2]^+$), 578.81 for complex **2** (theoretical m/z = 579.21 for $[Co(L^2)_2]^+$), and 500.99 (theoretical m/z = 501.49 for $[Co(L^3)_2]^+$) and 501.99 ($[Co(L^3)(HL^3)]^+$, theoretical m/z = 502.49) for complex **3**. The mass spectra of the complexes are shown in Fig. S7–S9 (ESI).†

In complex **1**, three signals for the aromatic protons of the 3-methoxysalicylaldehyde moiety were observed as a doublet at 6.90 ppm (J = 7.5 Hz), a doublet of doublets at 6.79 ppm (J = 1.5 Hz), and another doublet of doublets at 6.43 ppm (J = 7.5 Hz). The singlet at 8.03 ppm corresponded to the signals of benzylic protons (Ph–CH=N). The peaks at the range of 3.85–3.75 ppm may be assigned to the protons of the methoxy group of 3-methoxysalicylaldehyde and methylene protons attached to imine nitrogen atoms of the Schiff base units. The peaks at the range of 3.18–1.24 ppm may be assigned to the hydrogen atoms of the methylene protons of 3-amino-*N*,*N*-dimethylpropan-1-aminium units and methyl protons of $^+NHMe_2$ groups. In this complex, the methyl protons of $^+NHMe_2$ groups are not in the same environment due to an anisotropy effect of the benzene rings. The ^{1}H NMR spectrum of complex **1** is shown in Fig. S10.†

In complex **2**, two signals for the aromatic protons of the 3,5-dichlorosalicylaldehyde moiety were observed as singlets at 7.47 ppm (J = 1.5 Hz) and at 7.40 ppm (J = 1.5 Hz). The singlet at 8.50 ppm corresponded to the signals of benzylic protons (Ph–CH=N). Again, the peak at 7.40 ppm corresponded to the

Table 7 Theoretical in parenthesis and experimental values (in cm^{-1}) for representative IR bands for complexes **1–3**

Complexes	(C=N) Schiff base	N3/SCN	NH stretching
1	1625 (1619)	2023 (2018)	3293 (3281) and 3232 (3225)
2	1641 (1638)	2022 (2016)	3292 (3285)
3	1648 (1637)	2023 (2025) & 2065 (2070)	—

signals of protons attached to the N of the $^{+}NHMe_2$ group. The methylene protons of the 3-amino-*N*,*N*-dimethylpropan-1-aminium unit were observed at 3.18 ppm (J = 7.1 Hz). The methylene protons of *N*,*N*-dimethyl-1,2-diaminoethane and methyl protons of the $^{+}NHMe_2$ group were observed in the ranges of 2.91–2.05 ppm (J = 7.1 Hz). The other methyl protons of the NMe_2 group were observed in the ranges of 1.57–1.24 ppm (J = 7.1 Hz). The ^{1}H NMR spectrum of complex **2** is shown in Fig. S11.†

Concluding remarks

In this manuscript, we report the synthesis and X-ray characterization of three new cobalt complexes, with tridentate N_2O-donor Schiff base ligands. Complex **1** contains a distorted octahedral cobalt(III), being bonded to two imine nitrogen atoms and two phenolate oxygen atoms of the zwitterionic forms of two Schiff base moieties and two nitrogen atoms of two terminal azides, along with a non-coordinate perchlorate. The structure of complex **2** consists of a distorted octahedral cobalt(III), being bonded to one amine nitrogen atom, one imine nitrogen atom, and one phenolate oxygen atom of a deprotonated Schiff base in a meridional fashion, one imine nitrogen atom and one phenolate oxygen atom of the zwitterionic Schiff base, and an azide nitrogen atom, along with a non-coordinate perchlorate and lattice water molecules. The asymmetric unit of complex **3** contains two crystallographically independent cationic units containing cobalt(III) and one anionic unit containing cobalt(II). The cobalt(III) centers are more or less octahedral in both cationic units, being bonded by one amine nitrogen atom, one imine nitrogen atom, and one phenolate oxygen atom of the deprotonated Schiff base in a meridional fashion, one imine nitrogen atom and one phenolate oxygen atom of the zwitterionic Schiff base, and one thiocyanate nitrogen atom. The anionic part of the complex consists of a tetra-coordinated distorted tetrahedral cobalt(II), being coordinated by two thiocyanate nitrogen atoms and two chloride ions. Examination of the X-ray packing of complexes **1–3** and their HS analyses revealed the structure-directing role of the CH$\cdots$X (X = N, S, Cl) interactions. These were investigated using QTAIM and NCI plot analysis. Their combination is useful to characterize NCIs in real space. Although the individual interaction energies associated with these contacts are small, they are additive and can lead to a moderately strong stabilization of supramolecular synthons.

Finally, the advancements in structural diversity, intermolecular interaction studies, and the potential for tailored materials design showcase the significance of these complexes in advancing both fundamental knowledge and practical applications within the realm of coordination chemistry and beyond. Their flexible nature and unique features offer promising directions for future research and development, like catalysis, molecular design, and crystal engineering.

Conflicts of interest

The authors declare no conflict of interest.

Acknowledgements

Susovan Bera and Sudip Bhunia thank UGC, India for providing Junior Research Fellowship (JRF). A. F. is grateful to the Alexander von Humboldt Foundation for the J. C. Mutis Award. A. F. and R. G. M. acknowledge the financial support by the MICIU/AEI of Spain (project PID2020-115637GB-I00, FEDER funds).

References

1 B. De Clercq and F. Verpoort, *Macromolecules*, 2002, **35**, 8943–8947.
2 T. Opstal and F. Verpoort, *Angew. Chem., Int. Ed.*, 2003, **42**, 2876–2879.
3 B. De Clercq, F. Lefebvre and F. Verpoort, *Appl. Catal., A*, 2003, **247**, 345–364.
4 S. L. Lambert, C. L. Spiro, R. R. Gagne and D. N. Hendriekson, *Inorg. Chem.*, 1982, **21**, 68–72.
5 S. Brooker, *Coord. Chem. Rev.*, 2001, **222**, 33–56.
6 V. Amendola, L. Fabbrizzi, C. Mangano, P. Pallavicini, A. Poggi and A. Taglietti, *Coord. Chem. Rev.*, 2001, **219**, 821–837.
7 P. A. Vigato and S. Tamburini, *Coord. Chem. Rev.*, 2004, **248**, 1717–2128.
8 K. Ghosh, S. Pattanayak and A. Chakravorty, *Organometallics*, 1998, **17**, 1956–1960.
9 S. Chattopadhyay, M. G. B. Drew, C. Diaz and A. Ghosh, *Dalton Trans.*, 2007, 2492–2494.
10 S. Roy, A. Dey, P. P. Ray, J. Ortega-Castro, A. Frontera and S. Chattopadhyay, *Chem. Commun.*, 2015, **51**, 12974–12976.
11 S. Jana, B. K. Shaw, P. Bhowmik, K. Harms, M. G. B. Drew, S. Chattopadhyay and S. K. Saha, *Inorg. Chem.*, 2014, **53**, 8723–8734.
12 R. Biswas, C. Diaz, A. Bauzá, M. Barceló-Oliver, A. Frontera and A. Ghosh, *Dalton Trans.*, 2014, **43**, 6455–6467.
13 R. Biswas, Y. Ida, M. L. Baker, S. Biswas, P. Kar, H. Nojiri, T. Ishida and A. Ghosh, *Chem. - Eur. J.*, 2013, **19**, 3943–3953.
14 A. Bhattacharyya, P. K. Bhaumik, P. P. Jana and S. Chattopadhyay, *Polyhedron*, 2014, **78**, 40–45.
15 A. Bhattacharyya, B. N. Ghosh, S. Herrero, K. Rissanen, R. Jiménez-Aparicio and S. Chattopadhyay, *Dalton Trans.*, 2015, **44**, 493–497.
16 R. Biswas, S. Giri, S. K. Saha and A. Ghosh, *Eur. J. Inorg. Chem.*, 2012, 2916–2927.
17 R. Biswas, C. Diaz and A. Ghosh, *Polyhedron*, 2013, **56**, 172–179.
18 P. Ghorai, A. Chakraborty, A. Panja, T. K. Mondal and A. Saha, *RSC Adv.*, 2016, **6**, 36020–36030.
19 S. Mukherjee and P. S. Mukherjee, *Dalton Trans.*, 2013, **42**, 4019–4030.
20 S. C. Manna, S. Mistri, A. Patra, M. K. Mahish, D. Saren, R. K. Manne, M. K. Santra, E. Zangrand and H. Puschmann, *Polyhedron*, 2019, **171**, 77–85.
21 A. Bhunia, V. Bertolasi and S. C. Manna, *Appl. Organomet. Chem.*, 2020, **34**, e5424.
22 S. Chattopadhyay, P. Chakraborty, M. G. B. Drew and A. Ghosh, *Inorg. Chim. Acta*, 2009, **362**, 502–508.

23 S. Chattopadhyay, M. G. B. Drew and A. Ghosh, *Polyhedron*, 2007, **26**, 3513–3522.
24 M. Das, B. N. Ghosh, A. Valkonen, K. Rissanen and S. Chattopadhy, *Polyhedron*, 2013, **60**, 68–77.
25 S. Chattopadhyay, G. Bocelli, A. Cantoni and A. Ghosh, *Inorg. Chim. Acta*, 2006, **359**, 4441–4446.
26 K. Ghosh, M. G. B. Drew and S. Chattopadhyay, *Inorg. Chim. Acta*, 2018, **482**, 23–33.
27 K. Ghosh and S. Chattopadhyay, *Polyhedron*, 2019, **170**, 495–507.
28 K. Ghosh and K. Harms, *ChemistrySelect*, 2017, **2**, 8207–8220.
29 N. C. Jana, M. Patra, P. Brandão and A. Panja, *Inorg. Chim. Acta*, 2019, **490**, 163–172.
30 S. K. Dey and A. Mukherje, *Coord. Chem. Rev.*, 2016, **310**, 80–115.
31 K. Ghosh, K. Harms, A. Franconetti, A. Frontera and S. Chattopadhyay, *J. Organomet. Chem.*, 2019, **883**, 52–64.
32 S. Roy, S. Halder, K. Harms, P. P. Ray and S. Chattopadhyay, *New J. Chem.*, 2020, **44**, 1285–1293.
33 J. L. Dempsey, B. S. Brunschwig, J. R. Winkler and H. B. Gray, *Acc. Chem. Res.*, 2009, **42**, 1995–2004.
34 T. M. McCormick, B. D. Calitree, A. Orchard, N. D. Kraut, F. V. Bright, M. R. Detty and R. Eisenberg, *J. Am. Chem. Soc.*, 2010, **132**, 15480–15483.
35 W. R. McNamara, Z. Han, C. Yin, W. W. Brennessel, P. L. Holland and R. Eisenberg, *Natl. Acad. Sci. U.S.A.*, 2012, **109**, 15594–15599.
36 S. Kal, A. S. Filatov and P. H. Dinolfo, *Inorg. Chem.*, 2014, **53**, 7137–7145.
37 W. R. McNamara, Z. Han, P. J. Alperin, W. W. Brennessel, P. L. Holland and R. Eisenberg, *J. Am. Chem. Soc.*, 2011, **133**, 15368–15371.
38 V. Artero, M. Chavarot-Kerlidou and M. Fontecave, *Angew. Chem., Int. Ed.*, 2011, **50**, 7238–7266.
39 X. Li, W. Ge, S. Guo, J. Bai and W. hong, *Angew. Chem., Int. Ed.*, 2023, **62**, e202216819.
40 M. H.-Y. Chan and V. W.-W. Yam, *J. Am. Chem. Soc.*, 2022, **144**, 22805–22825.
41 A. S. Novikov, *Crystals*, 2022, **12**, 246.
42 W. L. Ping, J. S. Bo, Z. W. Feng, L. Y. Qi and Y. Gui, *Chin. Sci. Bull.*, 2013, **58**, 2733–2740.
43 D. Sadhukhan, A. Ray, G. Pilet, C. Rizzoli, G. M. Rosair, C. J. Gomez-García, S. Signorella, S. Bell and S. Mitra, *Inorg. Chem.*, 2011, **50**, 8326–8339.
44 C.-L. Hu and J.-G. Mao, *Coord. Chem. Rev.*, 2015, **288**, 1–17.
45 G. N. D. Francesco, A. Gaillard, I. Ghiviriga, K. A. Abboud and L. J. Murray, *Inorg. Chem.*, 2014, **53**, 4647–4654.
46 K. Kalyanasundaram and M. Gratzel, *Coord. Chem. Rev.*, 1998, **77**, 347–414.
47 S. Roy, M. G. B. Drew, A. Bauzá, A. Frontera and S. Chattopadhyay, *Dalton Trans.*, 2017, **46**, 5384–5397.
48 S. Mirdya, A. Frontera and S. Chattopadhyay, *CrystEngComm*, 2019, **21**, 6859–6868.
49 Y. Shen, N. Ma, L. Wu and H.-H. Song, *Inorg. Chim. Acta*, 2015, **429**, 51–60.
50 Y.-S. Yang, Y.-P. Yang, M. Liu, Q.-M. Qiu, Q.-H. Jin, J.-J. Sun, H. Chen, Y.-C. Dai and Q.-X. Meng, *Polyhedron*, 2015, **85**, 912–917.
51 S. Carboni, C. Gennari, L. Pignataro and U. Piarulli, *Dalton Trans.*, 2011, **40**, 4355–4373.
52 L. Wang, B. Song, S. Khalife, Y. Li, L.-J. Ming, S. Bai, Y. Xu, H. Yu, M. Wang, H. Wang and X. Li, *J. Am. Chem. Soc.*, 2020, **142**, 1811–1821.
53 G. Mahmoudi, A. Bauzá and A. Frontera, *Dalton Trans.*, 2016, **45**, 4965–4969.
54 C. A. Hunter and J. K. M. Sanders, *J. Am. Chem. Soc.*, 1990, **112**, 5525–5534.
55 S. K. Burley and G. A. Petsko, *Science*, 1985, **229**, 23–28.
56 K. S. Kim, P. Tarakeshwar and J. Y. Lee, *Chem. Rev.*, 2000, **100**, 4145–4185.
57 J. C. Ma and D. A. Dougherty, *Chem. Rev.*, 1997, **97**, 1303–1324.
58 K. S. Kim, J. Y. Lee, S. J. Lee, T.-K. Ha and D. H. Kim, *J. Am. Chem. Soc.*, 1994, **116**, 7399–7400.
59 P. Middya, M. Karmakar, R. M Gomila, M. G. B. Drew, A. Frontera and S. Chattopadhyay, *J. Chem.*, 2023, **47**, 9346–9363.
60 D. Quiñonero, C. Garau, C. Rotger, A. Frontera, P. Ballester, A. Costa and P. M. Deyà, *Angew. Chem., Int. Ed.*, 2002, **41**, 3389–3392.
61 M. Egli and S. Sarkhel, *Acc. Chem. Res.*, 2007, **40**, 197–205.
62 T. J. Mooibroek, P. Gamez and J. Reedijk, *CrystEngComm*, 2008, **10**, 1501–1515.
63 J. Ran and P. Hobza, *J. Chem. Theory Comput.*, 2009, **5**, 1180–1185.
64 M. Barceló-Oliver, C. Estarellas, A. García-Raso, A. Terrón, A. Frontera, D. Quiñonero, E. Molins and P. M. Deyà, *CrystEngComm*, 2010, **12**, 362–365.
65 M. Nishio, *CrystEngComm*, 2004, **6**, 130–156.
66 J. Xiao, P. Broz, A. W. Puri, E. Deu, M. Morell, D. M. Monack and M. Bogyo, *J. Am. Chem. Soc.*, 2013, **135**, 9130–9138.
67 S. Naskar, D. Mishra, R. J. Butcher and S. K. Chattopadhyay, *Polyhedron*, 2007, **26**, 3703–3714.
68 A. Bauzá, D. Quiñonero, P. M. Deyà and A. Frontera, *Chem. - Asian J.*, 2013, **8**, 2708–2713.
69 L. M. Salonen, M. Ellermann and F. Diederich, *Angew. Chem., Int. Ed.*, 2011, **50**, 4808–4842.
70 S. Jana, K. Harms, A. Bauzá, A. Frontera and S. Chattopadhyay, *Cryst. Growth Des.*, 2015, **15**, 257–267.
71 S. Cañellas, A. Bauzá, A. Lancho, A. Garcia-Raso, J. J. Fiol, E. Molins, P. Ballesterc and A. Frontera, *CrystEngComm*, 2015, **17**, 5987–5997.
72 G. M. Sheldrick, *Acta Crystallogr.*, 2015, **71A**, 3–8.
73 G. M. Sheldrick, *SADABS, V2014/5, Software for Empirical Absorption Correction*, University of Göttingen, Institute fur Anorganische Chemieder Universitat, Gottingen, Germany, pp. 1999–2003.
74 M. A. Spackman and D. Jayatilaka, *CrystEngComm*, 2009, **11**, 19–32.
75 F. L. Hirshfeld, *Theor. Chim. Acta*, 1977, **44**, 129–138.
76 H. F. Clausen, M. S. Chevallier, M. A. Spackman and B. B. Iversen, *New J. Chem.*, 2010, **34**, 193–199.

77 A. L. Rohl, M. Moret, W. Kaminsky, K. Claborn, J. J. McKinnon and B. Kahr, *Cryst. Growth Des.*, 2008, **8**, 4517–4525.
78 A. Parkin, G. Barr, W. Dong, C. J. Gilmore, D. Jayatilaka, J. J. McKinnon, M. A. Spackman and C. C. Wilson, *CrystEngComm*, 2007, **9**, 648–652.
79 M. A. Spackman and J. J. McKinnon, *CrystEngComm*, 2002, **4**(66), 378–392.
80 S. K. Wolff, D. J. Grimwood, J. J. McKinnon, D. Jayatilaka and M. A. Spackman, *Crystal Explorer 2.0*, University of Western Australia, Perth, Australia, 2007, **http://hirshfeldsurfacenet.blogspot.com**.
81 F. H. Allen, O. Kennard, D. G. Watson, L. Brammer, A. G. Orpen and R. J. Taylor, *J. Chem. Soc., Perkin Trans.*, 1987, **2**, S1–S19.
82 J. J. Kinnon, M. A. Spackman and A. S. Mitchell, *Acta Crystallogr.*, 2004, **B60**, 627–668.
83 R. Ahlrichs, M. Bar, M. Hacer, H. Horn and C. Komel, *Chem. Phys. Lett.*, 1989, **162**, 165–169.
84 S. Grimme, J. Antony, S. Ehrlich and H. Krieg, *J. Chem. Phys.*, 2010, **132**, 154104–154122.
85 F. Weigend, *Phys. Chem. Chem. Phys.*, 2006, **8**, 1057–1065.
86 J. Contreras-Garcia, E. R. Johnson, S. Keinan, R. Chaudret, J. P. Piquemal, D. N. Beratan and W. Yang, *J. Chem. Theory Comput.*, 2011, **7**, 625–632.
87 R. F. W. Bader, *Chem. Rev.*, 1991, **91**, 893–928.
88 T. Lu and F. Chen, *J. Comput. Chem.*, 2012, **33**, 580–592.
89 J. W. Humphrey, A. Dalke and K. Schulten, *J. Mol. Graphics*, 1996, **14**, 33–38.
90 K. Ghosh, M. G. B. Drew and S. Chattopadhyay, *Inorg. Chim. Acta*, 2018, **482**, 23–33.
91 S. Roy, P. K. Bhaumik, K. Harms and S. Chattopadhyay, *Polyhedron*, 2014, **75**, 57–63.
92 M. Das, B. N. Ghosh, A. Bauzá, K. Rissanen, A. Frontera and S. Chattopadhyay, *RSC Adv.*, 2015, **5**, 73028–73039.
93 S. Bhunia, R. M. Gomila, A. Frontera and S. Chattopadhyay, *Polyhedron*, 2022, **223**, 115910.
94 S. Bhattacharya, S. Roy, K. Harms, A. Bauzá, A. Frontera and S. Chattopadhyay, *Inorg. Chim. Acta*, 2016, **442**, 16–23.
95 K. Ghosh, K. Harms and S. Chattopadhyay, *Polyhedron*, 2017, **123**, 162–175.
96 J. Müller, C. Würtele, O. Walter and S. Schindler, *Angew. Chem., Int. Ed.*, 2007, **46**, 7775–7777.
97 D. Bandyopadhyay, M. Layek, M. Fleck, R. Saha and C. Rizzoli, *Inorg. Chim. Acta*, 2017, **461**, 174–182.
98 D. Cremer and J. A. Pople, *J. Am. Chem. Soc.*, 1975, **97**, 1354–1358.
99 K. Ghosh, T. Dutta, M. G. B. Drew, A. Frontera and S. Chattopadhyay, *Polyhedron*, 2020, **182**, 114432.
100 S. Sen, P. Talukder, S. K. Dey, S. Mitra, G. Rosair, D. L. Hughes, G. P. A. Yap, G. Pilet, V. Gramlich and T. Matsushita, *Dalton Trans.*, 2006, 1758–1767.
101 K. Kitaura and K. Morokuma, *Int. J. Quantum Chem.*, 1976, **10**, 325–340.
102 S. Jana, B. K. Shaw, P. Bhowmik, K. Harms, M. G. B. Drew, S. Chattopadhyay and S. K. Saha, *Inorg. Chem.*, 2014, **53**, 8723–8734.
103 M. Das, S. Chatterjee, K. Harms, T. K. Mondal and S. Chattopadhyay, *Dalton Trans.*, 2014, **43**, 2936–2947.
104 S. Khan, S. Jana, M. G. B. Drew, A. Bauzá, A. Frontera and S. Chattopadhyay, *RSC Adv.*, 2016, **6**, 61214–61220.
105 S. Chattopadhyay, M. S. Ray, S. Chaudhuri, G. Mukhopadhyay, G. Bocelli, A. Cantoni and A. Ghosh, *Inorg. Chim. Acta*, 2006, **359**, 1367–1375.
106 S. Khan, A. A. Masum, M. M. Islam, M. G. B. Drew, A. Bauzá, A. Frontera and S. Chattopadhyay, *Polyhedron*, 2017, **123**, 334–343.
107 A. Bhattacharyya, S. Sen, K. Harms and S. Chattopadhyay, *Polyhedron*, 2015, **88**, 156–163.
108 K. Ghosh, K. Harms, A. Bauzá, A. Frontera and S. Chattopadhyay, *CrystEngComm*, 2018, **20**, 7281–7292.
109 P. Bhowmik, A. Bhattacharyya, K. Harms, S. Sproules and S. Chattopadhyay, *Polyhedron*, 2015, **85**, 221–231.
110 N. Sarkar, M. G. B. Drew, K. Harms, A. Bauzá, A. Frontera and S. Chattopadhyay, *CrystEngComm*, 2018, **20**, 1077–1086.
111 A. Das, K. Bhattacharya, S. Giri and A. Ghosh, *Polyhedron*, 2017, **134**, 295–301.
112 A. Ray, G. M. Rosair, G. Pilet, B. Dede, C. J. Gómez- García, S. Signorella, S. Bellú and S. Mitra, *Inorg. Chim. Acta*, 2011, **375**, 20–30.
113 H. A. R. Pramanik, P. C. Paul, P. Mondal and C. R. Bhattacharjee, *J. Mol. Struct.*, 2015, **1100**, 496–505.
114 A. Saha, P. Majumdar and S. Goswami, *J. Chem. Soc., Dalton Trans.*, 2000, 1703–1708.
115 S. Thakurta, R. J. Butcher, G. Pilet and S. Mitra, *J. Mol. Struct.*, 2009, **929**, 112–119.
116 A. H. Kianfar, W. A. K. Mahmood, M. Dinari, M. H. Azarian and F. Z. Khafri, *Spectrochim. Acta, Part A*, 2014, **127**, 422–428.
117 L. Mandal and S. Mohanta, *Dalton Trans.*, 2014, **43**, 15737–15751.
118 A. K. Ghosh, M. Mitra, A. Fathima, H. Yadav, A. R. Choudhury, B. U. Nair and R. Ghosh, *Polyhedron*, 2016, **107**, 1–8.